A Methodology to Study Chemotaxis in 3-D Collagen Gels

Sergio Caserta
Dipartimento di Ingegneria Chimica dei Materiali e della Produzione Industriale, Università degli studi di Napoli Federico II, P.le V. Tecchio 80, 80125 Naples, Italy

CEINGE–Advanced Biotechnologies, Via Sergio Pansini, 5, 80131 Naples, Italy

Consorzio Interuniversitario Nazionale per la Scienza e Tecnologia dei Materiali (INSTM), UdR INSTM Napoli Federico II, P.le Tecchio, 80, 80125 Naples, Italy

Silvia Campello
Dept. of Experimental Neuroscience, IRCCS Fondazione Santa Lucia, 00143 Rome, Italy

Giovanna Tomaiuolo
Dipartimento di Ingegneria Chimica dei Materiali e della Produzione Industriale, Università degli studi di Napoli Federico II, P.le V. Tecchio 80, 80125 Naples, Italy

CEINGE–Advanced Biotechnologies, Via Sergio Pansini, 5, 80131 Naples, Italy

Luigi Sabetta
Dipartimento di Ingegneria Chimica dei Materiali e della Produzione Industriale, Università degli studi di Napoli Federico II, P.le V. Tecchio 80, 80125 Naples, Italy

Stefano Guido
Dipartimento di Ingegneria Chimica dei Materiali e della Produzione Industriale, Università degli studi di Napoli Federico II, P.le V. Tecchio 80, 80125 Naples, Italy

CEINGE–Advanced Biotechnologies, Via Sergio Pansini, 5, 80131 Naples, Italy

Consorzio Interuniversitario Nazionale per la Scienza e Tecnologia dei Materiali (INSTM), UdR INSTM Napoli Federico II, P.le Tecchio, 80, 80125 Naples, Italy

DOI 10.1002/aic.14164
Published online July 15, 2013 in Wiley Online Library (wileyonlinelibrary.com)

We present here an innovative experimental methodology for the quantitative investigation of chemotaxis in vitro by live imaging of cell movement in a reconstituted three-dimensional collagen gel. A well-defined chemoattractant gradient is generated by means of a novel direct viewing chamber having two compartments (separated by a membrane), one containing the chemoattractant solution, the other the cell-seeded collagen gel matrix. Cell migration is observed by means of a time-lapse motorized video-microscopy workstation equipped with an incubating system and quantified by image analysis techniques. Experimental results on three different cell lines (Jurkat, fibroblasts, and lymphocytes) are presented for the isotropic control case (no chemoattractant) and in presence of a concentration gradient. Cell motility data are in line with the concentration profile, both theoretically calculated from Fick's law and experimentally measured by epifluorescence microscopy. In particular, a transient peak in cell response was found, possibly due to cell membrane receptor saturation. © 2013 American Institute of Chemical Engineers *AIChE J*, 59: 4025–4035, 2013
Keywords: chemotaxis, diffusion, collagen gel, 3-D cell tracking, time-lapse microscopy, cell motility

Introduction

Chemotaxis, the preferential movement of cells toward a concentration gradient of a soluble chemical, plays an important role in physiological and pathological processes, such as tumor growth,[1,2] skin and mucosa wound healing[3] and morphogenesis,[4] and inflammation.[5] In the former case, it is well-known that cancer cells can migrate through both individual and collective cell-migration strategies.[6] Furthermore, it has been recently shown that diffusional instability[7] mechanisms can induce the separation of single or clustered cells from the main tumor body, which can then migrate toward the source of a nutrient, for example, a blood vessel, thus, invading wider areas and tissues. Fibroplasias, the phase of wound healing in which fibroblasts repopulate the wound, is generally believed to involve the stimulation and chemotactic

Correspondence concerning this article should be addressed to S. Caserta at sergio.caserta@unina.it.

attraction of fibroblasts by growth factors and photolytic fragments of extracellular matrix molecules generated within the wound by macrophages.[4,8] For maintenance of immunity and tolerance, organs and tissues of the organism are connected by migrating leukocytes, in particular lymphocytes. Understanding leukocyte migration is essential for many disorders and diseases, especially, in mucosa-lined tissues. Leukocytes adhere to the vascular endothelium, and subsequently, leave the circulation by transendothelial migration driven by chemoattractants (chemokines), a process known as diapedesis. Reversible adherence of leukocytes to endothelium, basement membranes, and other surfaces on which they crawl, is an essential event in the establishment of inflammation. Detailed analyses of migrating lymphocytes have been performed both *in vivo* and *in vitro* with the aim of increasing the knowledge about the molecular machineries that control chemokine gradient sensing and migration of immune cells. It was found that different migration mechanisms can be active in two-dimensional (2-D) and in three-dimensional (3-D), due to different roles of adhesion.[9]

Hence, the development of physiologically relevant *in vitro* assays to study cell motility and chemotaxis in a quantitative way is a topic of growing interest.[10] Due to the complexity of the cell response, a detailed quantitative chemotaxis assay requires a rigorous approach, based on the measurement of objective cell movement indices and on the application of transport phenomena concepts. For this reason, the analysis of such biological problems is nowadays within the core business of Chemical Engineering.[11]

Several experimental approaches have been proposed in the literature to investigate cell chemotaxis both qualitatively and quantitatively. Among the first commonly used cell migration assays, the Boyden chamber[12] and the under agarose assay[13] have the disadvantages that cell migration cannot be monitored as a function of time and that concentration gradients are not well-defined. Direct visualization chambers are considered the gold standard for investigating the dynamic behavior of cells migrating under a chemotactic gradient.[14] Microfluidic devices, usually fabricated in PolyDiMethylSiloxane (PDMS) by soft lithography,[15–18] have been recently proposed as a tool to observe cell behavior and motion under chemotaxis or interstitial flow conditions. Convective and diffusive transport can be decoupled using microfluidics agarose membranes; in addition, the effect of shear stress can be investigated by exposing the cells to static or pulsating flows.[19,20] Direct observation chambers where the chemoattractant solution is in contact with a 3-D gel containing cells have been also reported.[21,22] Two compartments, containing chemoattractant and cells, respectively, are connected side by side horizontally[23] in the Zigmond chamber or as concentric rings[24] in the Dunn chamber. A different technique[25] is based on gradient generation by producing patterns on the surface of a collagen gel via printing with a micropump that dispenses small droplets of solution at controlled rates.

An ideal *in vitro* assay of cell chemotaxis should be carried out in a tissue-like collagen or fibrin gel, allowing for cell tracking and imaging of the concentration gradient of the chemotactic factor (CF) within the (optically transparent) gel, and be relatively simple to set up with significant reproducibility. These criteria have been fulfilled in the *in vitro* assay of leukocyte chemotaxis reported by Moghe et al.,[26] in which cells are initially dispersed throughout the gel rather than concentrated on the filter surface as in the Boyden chamber, thus minimizing cell—cell interactions and cell alteration of the CF gradient. Furthermore, cell migration occurs over distances many times the cell dimension, as in physiological processes involving chemotaxis, and can be directly observed. Another advantage of this "free diffusion" assay is that the spatial CF concentration gradient decays over a few hours (typically 12–24 h), that is, enough time for the cells to spread and migrate[27] significantly. In a simple modification of this leukocyte chemotaxis assay reported by Tranquillo et al.[28] a gradient of similar steepness is generated for longer periods thus allowing to test slower cells, such as fibroblasts. This involves the placement of a barrier between the two halves of the chamber (one-half initially containing CF at uniform concentration), leaving a small opening at one end of the barrier that serves to geometrically (or dimensionally) constrain free diffusion. Hence, the passage of the diffusing molecules is hindered, thereby, slowing down the decay rate of the spatial gradient, which emanates radially outward from the opening.

The aim of the present work is the development of a novel direct-viewing chamber for chemotaxis studies, which allows one to overcome some of the limitations of the existing assays and is based on time-lapse microscopy with motorized sample positioning and stage incubation, coupled with image analysis techniques. Overall, our methodology provides an integration of features, which are not found altogether in other assays from the literature: live cell imaging with both low and high-resolution optics, a 3-D extracellular matrix, quantitative data analysis based on cell tracking, a well-characterized concentration gradient lasting for extended time periods, an autoclavable chamber simple to operate and including a control well.

In the assay presented in this work, a chemoattractant concentration gradient in a collagen gel sample seeded with cells was generated by diffusion trough a porous membrane. We analyzed migration of cells from an immortalized lymphocyte line (Jurkat), human peripheral lymphocytes, and fibrosarcoma epithelial cells under concentration gradients of different chemoattractants. The diffusion process of the latter was monitored by epifluorescence microscopy of Fluorescein IsoThioCyanate (FITC)-labeled dextran. Cell motion under the action of the chemoattractant gradient was followed by time-lapse video microscopy. Cell tracking was performed offline by image analysis and the results were expressed in terms of a chemotactic index.

Material and Methods

Chemotaxis chamber

The chamber was designed with the requirements of maintaining both cell viability and good optical quality over a time scale of 24 h. The chamber, shown in Figure 1, consists of two steel blocks (Part 1 and 2 in Figure 1) each glued on top of a microscope slide using a silicone adhesive. The blocks are separated by a porous membrane (0.22 μm pores, Millipore) and assembled together by two mounting screws. Part 1 in Figure 1 has two independent compartments: the first one (A) is used as the control well while the second one (B) is the reservoir of the chemoattractant solution. In Part 2, there is only one compartment (C) which is used for the cell seeded collagen gel. Once assembled the membrane separating chemoattractant (B) and gel (C) compartments is

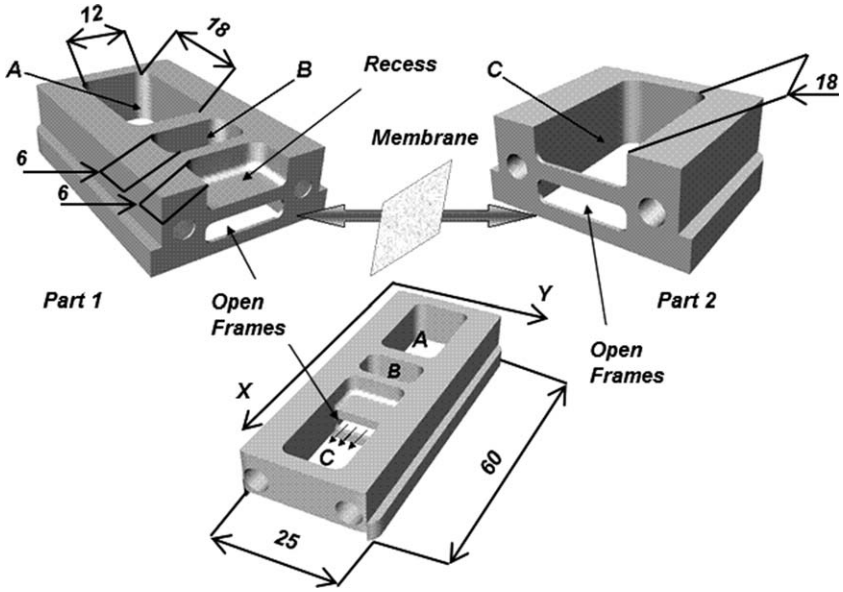

Figure 1. 3-D rendering of the chemiotaxis chamber.

sandwiched between the two rectangular open frames in Part 1 and 2, thereby, allowing chemoattractant diffusion from B to C. The diffusion can be considered one-dimensional along the x direction, as supported by the experimental finding of a constant concentration (see CF concentration profile measurement subsection) for any given value of x over the y and z range of interest, that is, far from the gel-air interface, where the sample is investigated.

At one side of Part 1 a recess, open at one side, extends the C compartment over the top part of the B compartment. The collagen level in the compartment C is made slightly higher than the open frame so as to completely fill the recess, with the advantage that possible lens effects due to the free interface of the gel in contact with the steel surface of the open frames near the membrane are avoided. This allows to image the sample region adjacent the membrane without optical distortions.

The A and C compartments are 12 mm $\times$ 18 mm, while the B compartment has a smaller size (12 mm $\times$ 6 mm) in order to minimize the amount of chemoattractant needed for each experiment. The open frame is 3 mm high along the vertical (z) direction, starting from the glass surface, and extends over the entire 12 mm of the C compartment width.

Preparation of chemotaxis assays

Collagen gels are prepared with the following composition (volume basis): Dulbecco's Modified Eagle Medium (DMEM) (2%), 0.1 M NaOH (13.2%), 10$\times$ minimum essential medium (10%), Fetal Bovine Serum (FBS) (6.7%), P/S (0.1%), L-glutamine (1%), and Vitrogen 100 collagen solution (67%, Celtrix Laboratories). The collagen concentration in the final solution was 2 mg/mL. It is worth mentioning that the matrix type or morphology, that is, fibers length and density, and matrix stiffness can also influence cell motility.[29,30] Matrix morphology can be influenced by changing the collagen concentration and the time and temperature of incubation during fibrillogenesis (e.g., polymerization could also be run, without cells, overnight at 4°C, leadings to thinner and longer fibres).

Cells preliminary suspended in DMEM with 10% FBS are added to the mixture in such a way that the initial cell concentration is between 10^3 and 10^4 cells/mL. Such a low cell concentration is chosen in order to minimize cell restructuring of the fibril orientation,[31] matrix degradation, or distortion of the chemoattractant concentration profile. The collagen solution is placed in the A and C compartments of the chamber, preliminarily sterilized in an autoclave. Collagen gelification is allowed to occur in a humidified incubator at 37°C, and final gel thickness is about 2 mm.

Time lapse microscopy

Microscope observations have been run using a video microscopy time lapse workstation.[32–34] The microscope (Zeiss Axiovert 200, 10$\times$ and 20$\times$ objectives) is equipped with a high sensitivity cooled CCD camera (Hamamtsu Orca AG) and motorized stage, focus (Marzhauser) and filter wheels (Prior) for automated 6-D Time Lapse imaging. The stage repositioning error (repeatability: < 1 μm, resolution: 0.01 μm, accuracy: ± 3 μm, data from the manufacturer), is below the optical resolution of our experiments, due to the pixel size (0.5–1.0 μm, depending on the optic used), and we can consider the overall planar repositioning error to be around 1 μm. The workstation is operated by means of a Labview control software. The microscope is also equipped with a home-made incubator allowing one to keep the sample temperature at 37 ± 0.1°C in a saturated moisture atmosphere with 5% CO_2. Preliminary tests showed no difference in morphological and physiological cell features between a bench top and our microscope incubator up to 48–72 h, depending on the cell line. During the experiments different fields of view were chosen for each collagen gel compartment of the chemotaxis chamber; each position was periodically scanned acquiring a z-stack of about 40 images at different focus position. Images were stored on hard drive for offline analysis. The time interval between consecutive acquisitions was chosen in the range 2–10 min (depending on cell speed) in order to allow accurate tracking of cell trajectories. The actual image acquisition time (measured in

milliseconds by the PC internal clock) was recorded and used for the post processing calculations.

Cell Culture

Jurkat cells

Jurkat cells are an immortalized line of T lymphocyte cells which are widely used to study acute T cell leukemia and T cell signaling. Jurkat cells are also useful because of their ability to produce interleukin 2, which is a chemokine involved in cell interactions and migration. The Jurkat cells used in our experiments were grown in Roswell Park Memorial Institute (RPMI) 1640 medium supplemented with 10% (v/v) FBS, sodium pyruvate 1%, nonessential aminoacids 1%, and antibiotics (50 units/mL penicillin and 50 μg/mL streptomycin). Cell culture was carried out in a humidified incubator at 37°C under an atmosphere of 5% CO_2 in air. The chemoattractants used during the chemotaxis experiments on Jurkat cells are Stromal cell-Derived Factor 1 (SDF)-1α/CXCL12 (PeproTech)[35] and Rantes/CCL5 (R&D),[36] at a concentration of 2.5 and 50 nM, respectively, in the chemoattractant (B) compartment of the cell.

Lymphocyte isolation

White blood cells were purified from peripheral blood from consenting healthy human volunteers using density gradient centrifugation. First, the leukocyte rich plasma was obtained by sedimentation from undiluted blood. Subsequently, separation of the different populations of white blood cells was performed by centrifugation with different gradients overlaid with the leukocyte rich plasma. The optimal separation of the mononuclear cells was obtained by the centrifugation of the leukocyte rich plasma overlaying the gradient containing 24 parts of 9.5% Ficoll and 10 parts of 34% Isopaque. The mononuclear leukocytes (95% Lymphocytes and 5% Monocytes) formed a monolayer band at the plasma-Ficoll-Isopaque interface and other blood cells migrated to the bottom of the tube. The separated mononuclear leukocytes responded to stimulation with phytohemagglutin and viability of all leukocytes was not affected by Ficoll-Isopaque separation. In the chemotaxis experiments we added SDF-1α[35] at a concentration $C_0 = 4.5$ nM in the B compartment of the cell.

Fibroblasts

HT1080 is an epithelial cell line of fibrosarcoma from connective tissue. This cell line presents a good cell motility, a significant morphological polarization and an excellent growth capacity that allows an adaptation to different experimental conditions. The cells are cultured in DMEM medium supplemented with 10% (v/v) FBS, sodium pyruvate 1% and antibiotics (50 units/mL penicillin and 50 μg/mL streptomycin) and maintained in a humidified incubator at 37°C under an atmosphere of 5% CO_2 in air. In chemotaxis experiments, we added 1 mL of FBS in the B compartment of the chamber,[37] and the collagen gel composition was modified by substituting FBS with an equal quantity of DMEM.

CF concentration profile measurements

To study chemoattractant diffusion a fluorescently labeled dextran (FITC-dextran from Sigma) of comparable molecular weight was used. The mean gray level, which is proportional to fluorescence intensity, was measured by confocal microscopy (Zeiss Pascal) as a function of time and position in order to characterize the propagation of the FITC-dextran front in the collagen gel. A preliminary calibration on gels with uniform FITC-dextran concentration was performed to convert intensity measurement to concentration values. A linear dependence was found in the entire concentration range examined (up to 100 μM), which was wider than the concentration range actually investigated in the chemotaxis tests.

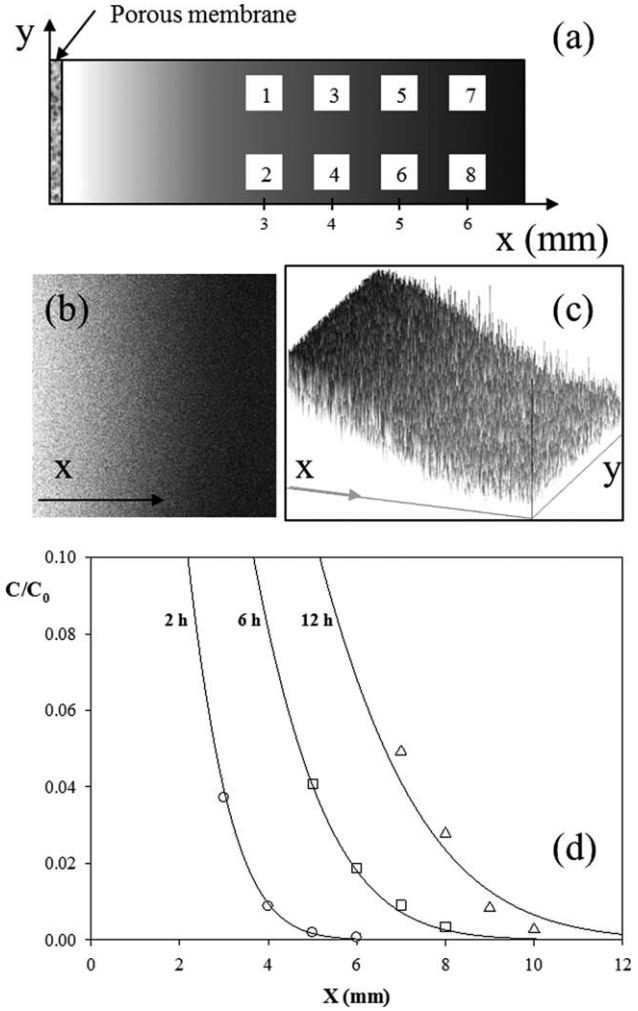

Figure 2. (a) Schematic of sample scanning areas during the diffusion characterization experiment; (b) Fluorescence image of FITC-dextran; (c) Surface plot of the fluorescence image; (d) Comparison of the concentration profile as experimentally determined from fluorescence intensity, and the calculation according to data fit at three different acquisition times.

In order to determine the diffusion coefficient of FITC-dextran in the chemotaxis chamber the mean grey level in eight fields of view arranged in pairs at gradually increasing distance from the porous membrane was measured as a function of time, for every x, y position three images were acquired at 10 different focus position along the z direction, in the range 20–2000 micron as measured from the surface of the glass. The distance of the fields of view from the membrane (along the x-axis) ranged from 3 to 6 mm. A schematic of the arrangement of the selected fields of view is shown in Figure 2a.

Measurements of the FITC–dextran gradients were made at 0.5, 1, 12, 15, and 24 h after loading the chemoattractant compartment. A typical image showing the fluorescence

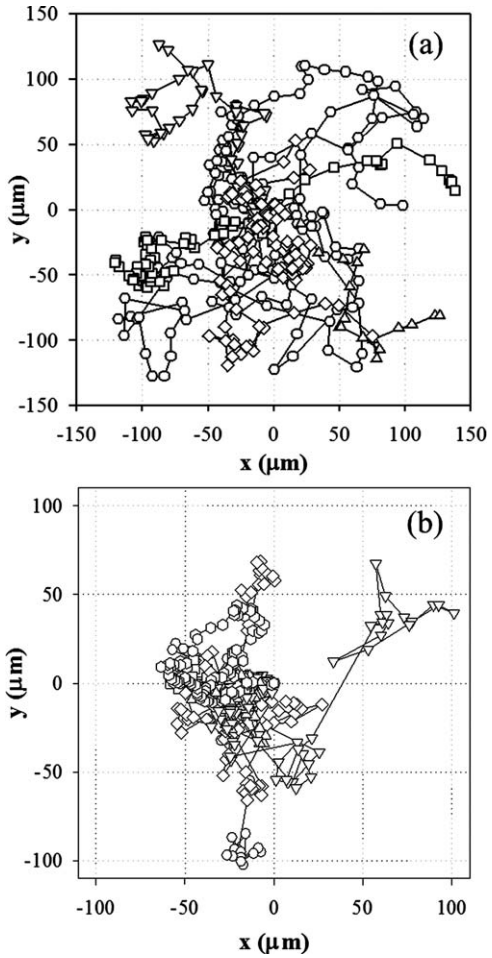

Figure 3. Jurkat cell trajectory projected on the *x, y* plane and reported to the same origin.

intensity gradient is presented in Figure 2b. A 3-D surface plot of the same image, where the light intensity is on the vertical axis, is shown in Figure 2c.

An analytical approximation of the concentration gradient was obtained by assuming the model of free Fickian diffusion (Eq. 1).

$$\frac{\partial C(x,t)}{\partial t} = D\frac{\partial^2 C(x,t)}{\partial x^2} \tag{1}$$

By invoking the symmetry of our assay chamber, we approximated the steady concentration at the membrane as $C_0/2$, where C_0 is the initial concentration in the chemoattractant compartment (compartment B in Figure 1). In addition, we assumed that the chemoattractant concentration was low enough not to influence mass transport, that is, the diffusion coefficient was constant,[38,39] and that the chamber walls were far from the membrane (i.e., $C|_{x\to\infty} = 0$). As the initial condition we set concentration to 0 in the entire diffusion chamber at $t = 0$ $\{C = 0,\ t = 0,\ x > 0\}$. The resulting well-known solution of Eq. 1, that is

$$C(x,t) = \frac{C_0}{2}\left[1 - \mathrm{erf}\left(\frac{x}{\sqrt{4Dt}}\right)\right] \tag{2}$$

was fit to experimental data to determine the diffusion coefficient of FITC-dextran, which turned out about 2×10^{-6} cm^2/sec, in good agreement with data from the literature.[26]

In Figure 2d, we reported the spatial concentration profile C, normalized with respect to the initial chemoattractant concentration in the reservoir (C_0), at three different timepoints. The concentration decreased exponentially with distance at each time. The continuous lines in Figure 2d corresponds to profiles calculated according to Eq. 2, while the symbols represent experimental data, measured as fluorescence intensity and converted to concentration according to the above mentioned calibration. The open frame of the chamber design inherently creates a 2-D diffusion gradient in the x and z directions. However, no significant differences in the concentration measurements have been observed among images acquired at the same x position, but different y and z, confirming the diffusive flow can be considered to be essentially along the x direction in our experimental conditions. The predicted profiles are in very good agreement with experimental measurements, in the range of concentration of interest in our experiments. It is worth mentioning that at long times the concentration at the wall opposite to the membrane departs from the initial zero value, and this is also accompanied by a decrease of the concentration at the membrane-collagen interface. So, at long times, the semi-infinite medium approximation (Eq. 2) starts to fail, as expected. The time when Eq. (2) fails to describe the actual concentration profile depends on the length of the chamber, that is, on the distance of the membrane from the opposite wall, the longer the chamber the wider the agreement.

The main aim of the FITC-Dextran diffusion tests was to provide experimental evidence that the chemotaxis chamber here presented is able to realize controlled and reproducible concentration profiles, which are in agreement with predictions from Fick's law. The molecular weight of the FITC-dextran (10 kDa) was comparable to that of the chemoattractants investigated in this work (about 8 kDa), so that a similar diffusion behavior can be assumed.[40,41] In the case of SDF-1α, (molecular weight 8.6 kDa) the measured value of the diffusion coefficient is 1.7×10^{-6} cm^2/s,[42] in good agreement with our estimate. This agreement rules out possible interactions between the diffusing chemoattractant molecules and the surrounding medium, that is, the collagen gel.

Cell tracking

Cell trajectory was measured by means of a semiautomated image analysis macro based on standard software libraries[43–45] (Image Pro Plus) that allows the user to identify each cell on the best focus layer at each time step (i.e., every 2–10 min, depending on cell line). Cell position arrays were then processed by a Matlab script in order to calculate mean squared displacements, average velocities and the chemotactic index.

The trajectory of each cell is represented by the sequence of the n positions of the cell center of mass as observed at given time steps. In a typical experiment, a cell number $M \approx 50$–100 was obtained in 3–6 fields of view. As already pointed out, a low cell concentration was chosen in this work, but it is worth mentioning that cells at higher concentrations can be tracked with the proposed method as well, provided the delay time between consecutive images, which is selected in the Time Lapse microscopy experiment, is low enough to avoid overlapping between trajectories of adjacent cells.

Cell movement in isotropic substrata can be described as a persistent random walk, and analyzed in terms of persistence

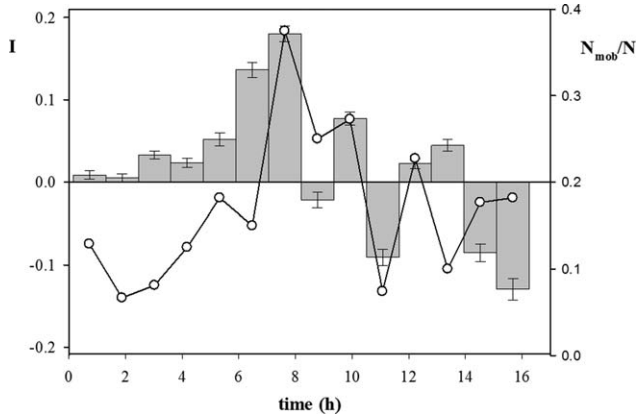

Figure 4. Analysis of motility for Jurkat cells under Rantes chemoattractant gradient ($C_0 = 50$nM).

time, root mean squared speed, and diffusion coefficient,[46] in analogy with Brownian particles.[47] Under a directional stimulus, like the chemoattractant gradient imposed in the compartment C of the chemotactic chamber, the space orientations are not equivalent and a directional bias in cell movement is expected. To quantitatively assess the degree of directionality in cell movement a chemotactic index (I) was calculated. Every experiment was divided in time intervals of about 1 h length, and for each of them we measured the net displacement (Δx_m) of every cell m in the direction of the chemoattractant source as the distance along the x direction between the cell positions at the end and the beginning of the time interval. For each time interval, we also calculated the length of the trajectory described by every cell (L_m) as the sum of all the displacements measured over two consecutive images. We then calculated the mth cell chemotaxis index over each time interval ($I_m = \Delta x_m/L_m$). The value of the average chemotaxis index during each time interval (I) was calculated as the average of I_m over the entire population of M cells, weighted according to the trajectory described by each cell (L_m) so that the cells describing the longer trajectories count the most (3):

$$I = \frac{\sum_{m=1}^{M} I_m L_m}{\sum_{m=1}^{M} L_m} \tag{3}$$

The chemotactic index ranges from $+1$ (trajectory fully oriented towards the source of the chemoattractant) to -1 (trajectory fully oriented in the opposite direction, corresponding the so called negative chemotaxis), whereas $I = 0$ corresponds to random movement.

Results

In this work, we report results from experiments performed on three different cell lines, in order to validate our assay. Cell behavior in the absence of external migration stimuli (compartment A) was also analyzed as a control.

Jurkat cells

A direct analysis of cell trajectories allows to preliminarily detect qualitative differences in cell behavior in presence or absence of chemoattractant. Time lapse images were acquired every 2 min and analyzed in order to detect cell positions, the trajectories of eight cells referred to the same origin and projected on the xy plane are plotted in Figure 3a. It can be noticed that the motion is random and no preferential direction is observed. In Figure 3b, the same chart is reported for 12 cells subjected to an SDF-1α (CXCL12) concentration gradient ($C_0 = 2.5$ nM). In this case, a preferential direction is evident, most of the cells migrating toward the chemoattractant source, that is, the negative x direction.

In a different experiment, Rantes (CCL5) with a concentration C_0 of 50 nM was used as a chemoattractant and cell motility was studied by trajectory reconstruction as previously described. We report here the analysis of a field of view located 1.5 mm from the membrane. Cell motility was tracked for about 16 h with time intervals of about 70 min, and for each time interval data have been averaged on some 30 cells. Visual inspection of the time-lapse videos showed that only a fraction of the cells did actually move during the experiment. A cell was considered mobile if its total displacement exceeded its own diameter. Based on this criterion, the fraction of mobile cells (N_{mob}/N) is reported as a function of time in Figure 4. It should be noticed that the range of mobile cells (10–30%) is in line with previous studies from the literature[48,49] on Jurkat cells in response to SDF-1α (the same applies to lymphocytes,[50–52] see next subsection). Furthermore, the motion of cells was not random in the presence of the chemoattractant. This can be assessed quantitatively using the chemotactic index. A positive value corresponds to cell movement in the direction of the chemoattractant source, while negative values correspond to movement in the opposite direction. In Figure 4, the bar chart reports the average chemotactic index, calculated at the same intervals as the fraction of mobile cells; the error bars shows the standard deviation of the cell population at each point. The evolution over time of the chemotactic index suggests that at short times cells are not yet affected by the presence of chemoattractant. At about 8 h after the beginning of the experiment a peak is found, reaching a value of about 0.18, while at later times the influence of the chemoattractant becomes vanishing, resulting in values of the chemotactic index oscillating around 0, which can be associated to random motility. The two data sets in Figure 4 show a correlation between the fraction of mobile cells and the chemotactic index. A possible interpretation of the transient nature of the chemotactic response is a saturation of the cell membrane receptors,[53,54] which should be reached at a local chemoattractant concentration close to the dissociation constant of the cells' receptor for the attractant.[55]

It is worth mentioning that a rough estimate of the order of magnitude of the chemoattractant diffusion coefficient can be obtained by dividing the squared distance of the distance from the membrane (1.5 mm) by the time we observe the effect of the chemoattractant gradient (450 min). This calculations gives a value of $D \approx 10^{-6}$ cm^2/s, in good agreement with the FITC-dextran measurement. This, however, should be regarded as a rather approximate argument, due to the dependence of the chemotaxis response on both chemoattractant concentration and gradient.

Lymphocytes

Lymphocyte motility was investigated by using SDF-1α as a chemoattractant with a concentration $C_0 = 4.5$ nM. In the

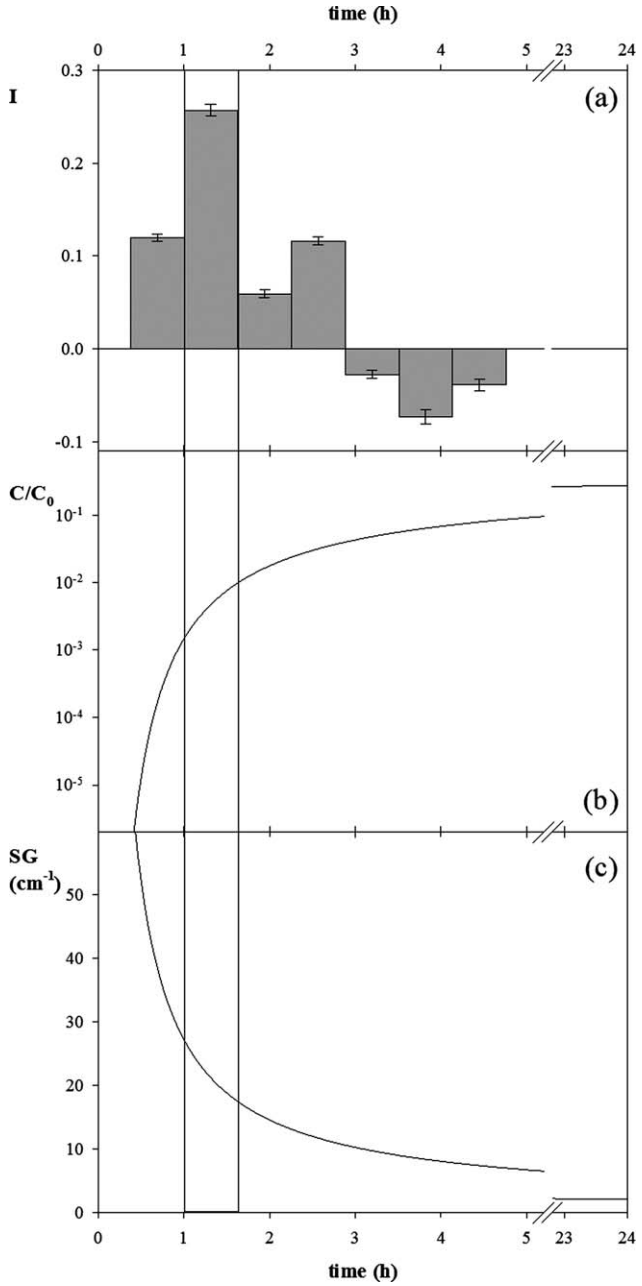

Figure 5. Analysis of motility for Lymphocyte cells under SDF-1α chemoattractant gradient (C_0 = 4.5nM).

time-lapse experiments shown in Figures 5 and 6 two fields of view, at 3.6 and 9.9 mm from the membrane, respectively, were observed. Data analysis was performed in the same way as previously described for Jurkat cells. In Figure 5a, we report the evolution of the chemotactic index over time for cells in the field of view at 3.6 mm from the membrane. As already observed for the Jurkat cells, the chemotaxis index shows a maximum about 60 min after the beginning of the experiment. The ability of a cell to sense a chemotactic gradient depends both on the chemoattractant concentration as well as the concentration gradient.[23] The latter can be expressed as a specific gradient (SG),[26] a scaled measure of the chemoattractant gradient steepness, having the dimension of an inverse length, which in our geometry can be calculated as follows

$$SG(x,t)=\frac{dc(x,t)}{dx}\frac{1}{c(x,t)}=\frac{\exp\left(-\frac{x^2}{4Dt}\right)}{\sqrt{\pi Dt}\left[1-erf\left(\frac{x}{\sqrt{4Dt}}\right)\right]} \quad (4)$$

Cell response can also depend on the differences in the fraction of receptors occupied between the front and the rear of a cell, this quantity being higher for nonlinear compared to linear gradients.[56] In Figure 5b, the evolution of the normalized concentration C/C_0 over time (1) is shown at $x = 3.6$ mm, based on the estimated value of $D = 2 \times 10^{-6}$ cm^2/sec, (it should be noticed that no significant differences would appear by using the value of D reported in the literature, which is1.7×10^{-6} cm^2/s).[42] In Figure 5c, SG time profile is reported for the same value of x. Comparing the peak in the chemotactic index with the C/C_0 and SG profiles, the maximum cellular response appears to be about 1 h from the

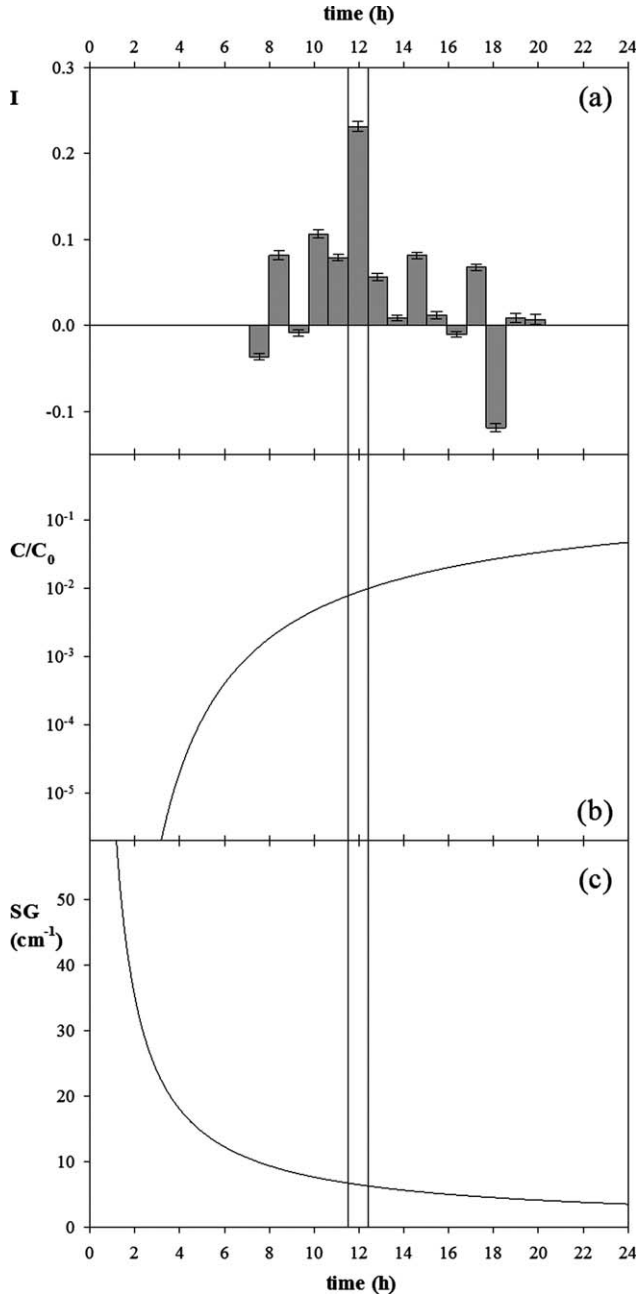

Figure 6. Analysis of motility for lymphocyte cells under SDF chemoattractant gradient (C_0= 4.5 nM).

beginning of the experiment, corresponding to a value of $C/C_0 \approx 0.005$, SG ≈ 20 cm^{-1}.

In Figure 6, the same analysis is shown for the field of view 9.9 mm from the membrane. In this case too we calculated the time profile of C/C_0 and SG, which are presented in Figures 6b and c, respectively. The highest value (Figure 6a) of the chemotactic index is found about 12 h from the beginning of the experiment, corresponding to a value of $C/C_0 \approx 0.008$, SG ≈ 7 cm^{-1}. The differences between the two fields of view can be further discussed by noting that in the case of Figure 6 (9.9 mm from the membrane) the SG reached a value ≈ 20 cm^{-1} after about 3.5 h, corresponding to a $C/C_0 < 10^{-5}$; in these conditions it is likely that chemoattractant concentration is too low to elicit a significant cell response. At later times (12 h), the increased concentration level would result in a significant cell response, even in the presence of a slightly reduced SG. As time goes on both the chemoattractant concentration and the SG increase further, while the SG reduces only slightly, approaching a plateau value, but at some point all the receptors will become saturated with ligands and the cell is unable to sense the gradient. This explanation is in agreement with previous works in the literature showing that cell ability to sense a concentration gradient is hindered at high chemoattractant concentration due to receptor saturation,[54,55] and that the cell response depends both on the concentration and SG value.[23] The value of the dissociation constant for SDF-1α on lymphocytes is estimated to be about 10 nM from the literature. This value can be considered in good agreement with dose-dependent chemotaxis response curves found by the Boyden assay,[57] where the maximum chemotactic response corresponds to a concentration of 10 nM in the lower chamber (the other tested values being 0.1, 1, or 100 nM). In our experiment, the concentration in the chemoattractant reservoir was 4.5 nM, and this value alone would suggest an agreement with Boyden data. However, our technique allows to monitor the dynamic evolution of cell motility and to compare it to the corresponding concentration profiles. By averaging the values from the two results reported in Figures 5 and 6, we can estimate that the peak in the chemotactic response corresponds to an actual concentration of about 0.03 nM, which is much lower than the concentration in the chemoattractant well, that can be considered in agreement to previous estimations of Kd from the literature. It should be mentioned that also in the Boyden assay the actual concentration surrounding the cells is lower than the value in the chemoattractant chamber, being variable over the time and space, even if at the filter midline the concentration and the gradient rapidly approach a value that keeps substantially constant for several hours.[58] This result could appear in disagreement with previous observations, reporting that the optimal chemotactic response is expected for concentration values near Kd,[23] showing a higher cell sensitivity to chemoattractant concentrations. It is expected that the conditions that provide optimal chemotaxis in one system may not be those that provide optimal chemotaxis to the same factor in a different system or to different chemotactic agents in the same assay system.[58,59] The analysis we performed differs from the Boyden assay not only because of differences in the chamber geometry, that result in differences in the concentration and SGs profiles[58] but also in terms of how the chemotactic response is analyzed. Like other visual assay, we monitor the dynamic behavior of cells, expressing quantitative parameters such as the chemotactic index, rather than monitoring the cell's ability to pass through a filter, comparing only the conditions at the beginning and at the end of the essay, like in Boyden. Furthermore, the concentration and SG profile imposed is typically not steady state, but evolves dynamically during the cell reaction (while the concentration rises, the SG rapidly drops), as reported in Figures 5 and 6 for our chamber, or by Lauffenburger and Zigmond[58] for other assays. It should be noticed, however, that the dependence of the chemotactic index on concentration and concentration gradient is still to be elucidated,[40] due to the complexity of the problem, different results obtained using different techniques can be expected to be different.

As before, a rough estimate of the diffusion coefficient can be obtained by dividing the squared characteristic length, that is, the distance between the two fields of view, by the characteristic time, that is, the observed delay time between

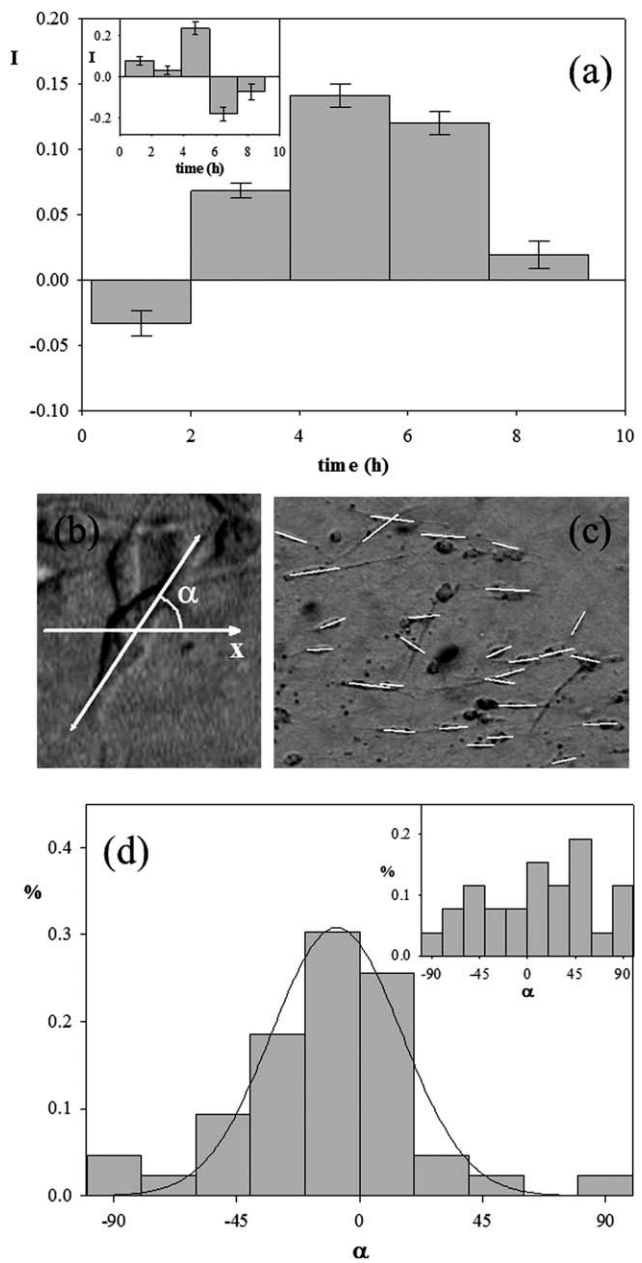

Figure 7. Analysis of motility for fibroblast under FBS chemoattractant gradient.

the two peaks. As already pointed out, the unknown dependence of the chemotaxis response on both SG and C makes this estimate not really straightforward, and can explain the difference between the estimated value of $\approx 10^{-5}$ cm^2/s and the measured value of the diffusion coefficient.

Fibroblasts

For the HT1080 cell line we used FBS as a chemoattractant. In Figure 7a, we report the chemotactic index as a function of time. For each time interval the measurement of about 40 cells was averaged, and the error bars correspond to the standard deviation of each population. As before, the chemotactic index grows up to a maximum, than goes back to a baseline value around 0. For comparison, in the inset of Figure 7a, the chemotactic index is shown for a control sample (i.e., in absence of chemotactic gradient) and no significant trend is observed. Once again, the peak in the chemotactic index is related to an increase in the fraction of mobile cells (data not shown for the sake of brevity).

For fibroblasts and other tissue cells with much slower migration speed and more polarized morphologies than Jurkat or lymphocytes the chemotactic cell response can be also quantified in terms of cell orientation.[28] The elongation of the cell body in the direction of the membrane up to the gradient of chemoattractant concentration (cell polarization) can be measured by image analysis, as shown in Figure 7b. In Figure 7c, a typical sample image is reported, where the cell major axis was manually overlaid. The measurement of the cell orientation angle α was performed on a z-stack acquired at the end of the experiment, that is, about 10 h from the start, for a population of about 50 cells. The distribution of the cell orientation angle is reported in Figure 7d. The distribution is well peaked around the gradient orientation ($\alpha = 0$) and in good agreement with a Gaussian fit ($R^2 = 0.94$), displayed as a continuous line. Polarized light observation of the collagen gel shows no preferential fiber orientation, thus confirming that cell polarization is induced by the chemotactic gradient and not by contact guidance.[60] As a further check, we measured the orientation distribution in the absence of chemoattractant gradient (see the inset of Figure 7d), and, as expected, in this case no preferential orientation is observed.

Conclusions

In conclusion, in this work, we present an innovative methodology for the experimental investigation of chemotaxis *in vitro* by time-lapse live cell imaging of cell movement under a controlled gradient of a chemoattractant in a direct viewing chamber. The latter is made of two compartments separated by a membrane allowing chemoattractant diffusion from the reservoir to the 3-D cell seeded collagen matrix and is autoclavable and reusable. The concentration profile can be experimentally quantified by fluorescence microscopy. The chamber allows comparing the results with a control sample, not subjected to any chemotactic gradient. The advantage is the ability to test both samples in the same experiment using the two wells of the chemotaxis chamber. The setup is easy to use, versatile and allows one to study chemotaxis on individual or clustered cells.

We validated our assay by three different case studies where Jurkat, lymphocyte, and fibroblast cells where stimulated by different chemoattractant gradients. In all cases, cell concentration was low enough to avoid possible degradation of the collagen matrix and distortion of the concentration gradient. The data have been analyzed by measuring the directionality of cell migration in terms of quantitative parameters, such as the chemotactic index. The proposed assay proved to be valid to investigate cell motility in random condition and under the presence of a chemotactic gradient, both in the case of fast moving (like white blood cells) and slow moving (like fibroblasts) cells. In all the cases investigated, we showed that cell response is transient, with a maximum corresponding to the onset of the chemotactic gradient in the field of view, likely due to cell membrane receptor saturation in agreement with previous studies. The motility data are in good agreement with the predicted concentration profile from Fick's law. The concentration value corresponding to the peak in the chemotactic index is significantly below the Kd value, as it could be expected from previous results from the literature. This discrepancy can be attributed to the fact that our assay is intrinsically transient both because the concentration profile and SG evolve in time, and because, like in other visual assays, cell behavior is monitored dynamically, rather than limiting to compare their position at the beginning and at the end of the test. The dependence of the cell motility on concentration and concentration gradient is still to be elucidated. The experimental approach here presented can be considered a valid instrument to quantitatively correlate the concentration profile with cell motility parameters.

Acknowledgments

The authors would like to thank Prof. Antonella Viola who provided biological support and useful discussions and suggestions. Fabio Raffone is gratefully acknowledged for the experimental support during his master thesis. Antonio Perazzo analysed the images for the FITC-dextran diffusion text during his bachelor thesis. Financial support from the Italian Ministry of Research (PRIN 2006, prot. 2006099155 and PRIN 2008, prot. 2008W3WBMH) is gratefully acknowledged. This study is related to the activity of the European network action COST MP1106 "Smart and green interfaces—from single bubbles and drops to industrial, environmental and biomedical applications." Silvia Campello is presently funded by the Italian Ministry of Health (GR-2009-1606827) and the AIRC program MyFAG (MFAG-12120).

Literature Cited

1. Vital-Lopez FG, Armaou A, Hutnik M, Maranas CD. Modeling the effect of chemotaxis on Glioblastoma Tumor Progression. *AIChE J*. 2011;57(3):778–792.
2. Hughes-Alford S, Lauffenburger D. Quantitative analysis of gradient sensing: towards building predictive models of chemotaxis in cancer. *Curr Opin Cell Biol*. 2012;24(2):284–291.
3. Clark RAF. Wound repair: overview and general considerations. In: Clark RAF, editor. The Molecular and Cellular Biology of Wound Repair, 2nd ed. New York: Plenum Press 1996:1–50.
4. Reddi AH. Bone morphogenetic proteins: an unconventional approach to isolation of first mammalian morphogens. *Cytokine Growth Factor Rev*. 1997;8(1):11–20.
5. Coussens LM, Werb Z. Inflammation and cancer. *Nature*. 2002; 420(6917):860–867.
6. Friedl P, Wolf K. Tumour-cell invasion and migration: diversity and escape mechanisms. *Nat Rev Cancer*. 2003;3(5):362–374.
7. Cristini V, Frieboes HB, Gatenby R, Caserta S, Ferrari M, Sinek J. Morphologic instability and cancer invasion. *Clin Cancer Res*. 2005; 11(19 Pt 1):6772–6779.

8. McCarthy JB, Iida J, Furcht LT. Mechanisms of parenchymal cell migration into wounds. In: Clark RAF, editor. The Molecular and Cellular Biology of Wound Repair, 2nd ed. New York: Plenum Press 1996:373–390.
9. Lämmermann T, Bader BL, Monkley SJ, Worbs T, Wedlich-Söldner R, Hirsch K, Keller M, Förster R, Critchley DR, Fässler R, Sixt M. Rapid leukocyte migration by integrin-independent flowing and squeezing. *Nature*. 2008;453(7191):51–55.
10. Wong W. Focus issue: a cell's sense of direction. *Sci Signal*. 2012; 5(213):1–2.
11. Ottino J. Chemical engineering in a complex world: grand challenges, vast opportunities. *AIChE J*. 2011;57(7):1654–1668.
12. Boyden S. The chemotactic effect of mixtures of antibody and antigen on polymorphonuclear leucocytes. *J Exp Med*. 1962;115: 453–466.
13. Nelson RD, Quie PG, Simmons RL. Chemotaxis under agarose: a new and simple method for measuring chemotaxis and spontaneous migration of human polymorphonuclear leukocytes and monocytes. *J Immunol*. 1975;115(6):1650–1656.
14. Muinonen-Martin AJ, Veltman DM, Kalna G, Insall RH. An improved chamber for direct visualisation of chemotaxis. *PLoS One*. 2010;5(12):1–9.
15. Bonvin C, Overney J, Shieh AC, Dixon JB, Swartz MA. A multichamber fluidic device for 3D cultures under interstitial flow with live imaging: development, characterization, and applications. *Biotechnol Bioeng*. 2010;105(5):982–991.
16. Lin F. A microfluidics-based method for analyzing leukocyte migration to chemoattractant gradients. Methods in Enzymology, Chemokines, Part B, Vol. 461. San Diego: Elsevier Academic Press Inc, 2009:333–347.
17. Li Jeon N, Baskaran H, Dertinger SKW, Whitesides GM, Van De Water L, Toner M. Neutrophil chemotaxis in linear and complex gradients of interleukin-8 formed in a microfabricated device. *Nat Biotechnol*. 2002;20(8):826–830.
18. Tomaiuolo G, Rossi D, Caserta S, Cesarelli M, Guido S. Comparison of two flow-based imaging methods to measure individual red blood cell area and volume. *Cytometry A*. 2012;81(12): 1040–1047.
19. Shao JB, Wu L, Wu JZ, Zheng YH, Zhao H, Jin QH, Zhao JL. Integrated microfluidic chip for endothelial cells culture and analysis exposed to a pulsatile and oscillatory shear stress. *Lab Chip*. 2009; 9(21):3118–3125.
20. Haessler U, Kalinin Y, Swartz M, Wu M. An agarose-based microfluidic platform with a gradient buffer for 3D chemotaxis studies. *Biomed Microdevices*. 2009;11(4):827–835.
21. Friedl P, Bröcker EB. Reconstructing leukocyte migration in 3D extracellular matrix by time-lapse videomicroscopy and computer-assisted tracking. *Methods Mol Biol*. 2004;239:77–90.
22. Sixt M, Lämmermann T. In vitro analysis of chemotactic leukocyte migration in 3D environments. *Methods Mol Biol*. 2011;769:149–165.
23. Zigmond SH. Ability of polymorphonuclear leukocytes to orient in gradients of chemotactic factors. *J Cell Biol*. 1977;75(2 Pt 1):606–616.
24. Zicha D, Dunn G, Brown A. A new direct-viewing chemotaxis chamber. *J Cell Sci*. 1991;99 (Pt 4):769–775.
25. Rosoff WJ, McAllister R, Esrick MA, Goodhill GJ, Urbach JS. Generating controlled molecular gradients in 3D gels. *Biotechnol Bioeng*. 2005;91(6):754–759.
26. Moghe PV, Nelson RD, Tranquillo RT. Cytokine-stimulated chemotaxis of human neutrophils in a 3-D conjoined fibrin gel assay. *J Immunol Methods*. 1995;180(2):193–211.
27. Tomasek JJ, Hay ED. Analysis of the role of microfilaments and microtubules in acquisition of bipolarity and elongation of fibroblasts in hydrated collagen gels. *J Cell Biol*. 1984;99(2):536–549.
28. Knapp DM, Helou EF, Tranquillo RT. A fibrin or collagen gel assay for tissue cell chemotaxis: assessment of fibroblast chemotaxis to GRGDSP. *Exp Cell Res*. 1999;247(2):543–553.
29. Dimilla P, Quinn J, Albelda S, Lauffenburger D. Measurement of individual cell-migration parameters for human tissue-cells. *AIChE J*. 1992;38(7):1092–1104.
30. Zaman MH, Trapani LM, Sieminski AL, Siemeski A, Mackellar D, Gong H, Kamm RD, Wells A, Lauffenburger DA, Matsudaira P. Migration of tumor cells in 3D matrices is governed by matrix stiffness along with cell-matrix adhesion and proteolysis. *Proc Natl Acad Sci USA*. 2006;103(29):10889–10894.
31. Knapp D, Tower T, Tranquillo R, Barocas V. Estimation of cell traction and migration in an isometric cell traction assay. *AIChE J*. 1999;45(12):2628–2640.
32. Buonomo R, Giacco F, Vasaturo A, Caserta S, Guido S, Pagliara V, Garbi C, Mansueto G, Cassese A, Perruolo G, Oriente F, Miele C, Beguinot F, Formisano P. PED/PEA-15 controls fibroblast motility and wound closure by ERK1/2-dependent mechanisms. *J Cell Physiol*. 2012;227(5):2106–2116.
33. Silano M, Vincentini O, Luciani A, Felli C, Caserta S, Esposito S, Villella VR, Pettoello-Mantovani M, Guido S, Maiuri L. Early tissue transglutaminase-mediated response underlies K562(S)-cell gliadin-dependent agglutination. *Pediatr Res*. 2012;71:532–538.
34. D'Argenio G, Mazzone G, Tuccillo C, Ribecco MT, Graziani G, Gravina AG, Caserta S, Guido S, Fogliano V, Caporaso N, Romano M. Apple polyphenols extract (APE) improves colon damage in a rat model of colitis. *Dig Liver Dis*. 2012;44(7):555–562.
35. Campello S, Lacalle RA, Bettella M, Mañes S, Scorrano L, Viola A. Orchestration of lymphocyte chemotaxis by mitochondrial dynamics. *J Exp Med*. 2006;203(13):2879–2886.
36. Magrini E, Szabò I, Doni A, Cibella J, Viola A. Serotonin-mediated tuning of human helper T cell responsiveness to the chemokine CXCL12. *PLoS One*. 2011;6(8):1–10.
37. Lucena S, Sanchez EE, Perez JC. Anti-metastatic activity of the recombinant disintegrin, r-mojastin 1, from the Mohave rattlesnake. *Toxicon*. 2011;57(5):794–802.
38. Jonas A, De Luca A, Pesce G, Rusciano G, Sasso A, Caserta S, Guido S, Marrucci G. Diffusive mixing of polymers investigated by Raman microspectroscopy and microrheology. *Langmuir*. 2010; 26(17):14223–14230.
39. De Luca AC, Rusciano G, Pesce G, Caserta S, Guido S, Sasso A. Diffusion in polymer blends by Raman microscopy. *Macromolecules*. 2008;41(15):5512–5514.
40. Walker GM, Sai JQ, Richmond A, Stremler M, Chung CY, Wikswo JP. Effects of flow and diffusion on chemotaxis studies in a microfabricated gradient generator. *Lab Chip*. 2005;5(6):611–618.
41. Lin F, Butcher EC. T cell chemotaxis in a simple microfluidic device. *Lab Chip*. 2006;6(11):1462–1469.
42. Veldkamp CT, Ziarek JJ, Su JD, Basnet H, Lennertz R, Weiner JJ, Peterson FC, Baker JE, Volkman BF. Monomeric structure of the cardioprotective chemokine SDF-1/CXCL12. *Protein Sci*. 2009;18(7): 1359–1369.
43. Caserta S, Simeone M, Guido S. Shear banding in biphasic liquid-liquid systems. *Phys Rev Lett*. 2008;100(13):1–4.
44. Pommella A, Caserta S, Guida V, Guido S. Shear-induced deformation of surfactant multilamellar vesicles. *Phys Rev Lett*. 2012;108(13): 1–4.
45. Caserta S, Guido S. Vorticity banding in biphasic polymer blends. *Langmuir*. 2012;28(47):16254–16262.
46. Dickinson RB, Tranquillo RT. Optimal estimation of cell movement indices from the statistical analysis of cell tracking data. *AIChE J*. 1993;39(12):1995–2010.
47. Biondi S, Quinn J. Direct observation of hindered brownian-motion. *AIChE J*. 1995;41(5):1324–1328.
48. Zheng Y, Kong Y, Goetzl EJ. Lysophosphatidic acid receptor-selective effects on Jurkat T cell migration through a Matrigel model basement membrane. *J Immunol*. 2001;166(4):2317–2322.
49. Pelletier AJ, van der Laan LJW, Hildbrand P, Siani MA, Thompson DA, Dawson PE, Torbett BE, Salomon DR. Presentation of chemokine SDF-1 alpha by fibronectin mediates directed migration of T cells. *Blood*. 2000;96(8):2682–2690.
50. Komai-Koma M, Gracie JA, Wei XQ, Xu DM, Thomson N, McInnes IB, Liew FY. Chemoattraction of human T cells by IL-18. *J Immunol*. 2003;170(2):1084–1090.
51. Franitza S, Alon R, Lider O. Real-time analysis of integrin-mediated chemotactic migration of T lymphocytes within 3-D extracellular matrix-like gels. *J Immunol Methods*. 1999;225(1–2):9–25.
52. Franitza S, Hershkoviz R, Kam N, Lichtenstein N, Vaday GG, Alon R, Lider O. TNF-alpha associated with extracellular matrix fibronectin provides a stop signal for chemotactically migrating T cells. *J Immunol*. 2000;165(5):2738–2747.
53. Haugh JM, Schneider IC. Effectiveness factor for spatial gradient sensing in living cells. *Chem Eng Sci*. 2006;61(17):5603–5611.
54. Schneider IC, Haugh JM. Quantitative elucidation of a distinct spatial gradient-sensing mechanism in fibroblasts. *J Cell Biol*. 2005; 171(5):883–892.
55. Herzmark P, Campbell K, Wang F, Wong K, El-Samad H, Groisman A, Bourne HR. Bound attractant at the leading vs. the trailing edge determines chemotactic prowess. *Proc Natl Acad Sci USA*. 2007;104(33):13349–13354.

56. Wang SJ, Saadi W, Lin F, Nguyen CMC, Jeon NL. Differential effects of EGF gradient profiles on MDA-MB-231 breast cancer cell chemotaxis. *Exp Cell Res*. 2004;300(1):180–189.
57. Jinquan T, Quan S, Jacobi HH, Madsen HO, Glue C, Skov PS, Malling HJ, Poulsen LK. CXC chemokine receptor 4 expression and stromal cell-derived factor-1 alpha-induced chemotaxis in CD4(+) T lymphocytes are regulated by interleukin-4 and interleukin-10. *Immunology*. 2000;99(3):402–410.
58. Lauffenburger DA, Zigmond SH. Chemotactic factor concentration gradients in chemotaxis assay systems. *J Immunol Methods*. 1981;40(1): 45–60.
59. Nelson RD, McCormack RT, Fiegel VD, Simmons RL. Chemotactic deactivation of human neutrophils: evidence for nonspecific and specific components. *Infect Immun*. 1978;22(2):441–444.
60. Guido S, Tranquillo RT. A methodology for the systematic and quantitative study of cell contact guidance in oriented collagen gels. Correlation of fibroblast orientation and gel birefringence. *J Cell Sci*. 1993;105 (Pt 2):317–331.

Manuscript received Nov. 2, 2012, and revision received May 6, 2013.